

Reinforcement learning for robust dynamic metabolic control

Sebastián Espinel-Ríos^{1*}, River Walser², Dongda Zhang³

¹ Biomedical Manufacturing Program, Commonwealth Scientific and Industrial Research Organisation, Clayton, Australia

² Basis Independent Brooklyn, New York, United States

³ Department of Chemical Engineering, University of Manchester, Manchester, United Kingdom

* **Correspondance.** Email: sebastian.espinelrios@csiro.au

Abstract

Dynamic metabolic control can enhance bioprocess flexibility and expand the available optimization degrees of freedom via real-time modulation of metabolic enzyme expression. This allows target metabolic fluxes to be dynamically tuned throughout the process. However, identifying optimal dynamic control policies is challenging due to the presence of potential metabolic burden, cytotoxic effects, and the generally high-dimensional solution space, making exhaustive experimentation impractical. Here, we propose an approach based on reinforcement learning to derive optimal dynamic metabolic control policies by allowing an agent or controller to interact with a surrogate dynamic model *in silico*. To incorporate and test robustness, we apply domain randomization, enabling the controller to generalize across system uncertainties. Our approach provides an alternative to conventional model-based control such as model predictive control, which requires differentiating the models with respect to decision variables; an often impractical task when dealing with complex stochastic, nonlinear, stiff, or piecewise-defined dynamics. In contrast, our approach only requires forward integration, making the task computationally much simpler with off-the-shelf solvers. We demonstrate our approach with a case study on the dynamic control of acetyl-CoA carboxylase in *Escherichia coli* for fatty acid biosynthesis. The derived dynamic metabolic control policies outperform static control, achieving up to 40 % higher titers while remaining robust under uncertainty.

KEYWORDS: reinforcement learning, dynamic metabolic control, stochastic control, enzyme expression, fatty acid biosynthesis.

1 Introduction

Advanced bioprocessing often involves engineering cellular metabolic networks to introduce new pathways or optimize the efficiency of existing ones (Volk et al. 2023). This is typically achieved through genetic engineering strategies, such as inserting, deleting, downregulating, or overexpressing metabolic enzymes. Because metabolic enzymes catalyze reactions within cells, their concentrations directly determine reaction rates. Thus, modulating enzyme expression offers a targeted means for precise control over metabolic fluxes, thereby making it possible to maximize production efficiency in bioprocesses by reconfiguration of metabolic networks (cf. e.g. (Espinel-Ríos & Avalos 2024; Espinel-Ríos, Behrendt, et al. 2024; Espinel-Ríos, Morabito, et al. 2024)).

Control of enzyme expression typically relies on responding to specific signals, leading to two distinct control paradigms: static and dynamic (Brockman & Prather 2015; Hartline et al. 2021). Static control involves a constant induction level, offering operational simplicity but significantly limiting dynamic optimization flexibility. Such fixed expression levels are often engineered by selecting suitable promoters or adjusting gene copy numbers. In contrast, under ideal conditions, dynamic metabolic control continuously and reversibly modulates enzyme expression, enabling greater operational flexibility and providing access to a broader range of metabolic modes to exploit the full potential of microbial cell factories.

A central challenge in metabolic control is identifying optimal enzyme modulation policies that maximize product pathway efficiency while minimizing cytotoxicity and intrinsic metabolic burdens. Excessive or uncontrolled enzyme expression can rapidly arrest growth by depleting cellular resources or causing unintended cytotoxic effects (cf. e.g., (Hoffman et al. 2025; Ohkubo et al. 2024)). Therefore, higher enzyme expression levels do not necessarily translate into increased production efficiency.

While static control policies can, in principle, be simpler to derive, even through trial and error, elucidating optimal dynamic policies is significantly more challenging. This complexity arises from inherent nonlinearities (e.g., steep activation and deactivation kinetics), multi-scale dynamics, delayed responses, piecewise or switch-like functions triggered by specific cellular events, and the presence of system uncertainties (e.g., stochastic gene expression, process variability, and external disturbances) commonly encountered in engineered microbial cell factories and bioprocesses (Glass et al. 2021; Olsson et al. 2022; Oyarzún & Chaves 2015; Pal & Dhar 2024; Zhang et al. 2006). Consequently, dynamic metabolic control represents a nontrivial *nonlinear, stochastic, and dynamic* control problem. To address this challenge, we propose reinforcement learning (RL) (Ding et al. 2020; Sutton & Barto 2018), a machine-learning-based feedback control approach, to derive optimal dynamic policies for enzyme expression regulation in response to time-varying metabolic states, aiming to maximize production efficiency under uncertainty.

Traditional model-based dynamic control strategies, such as model predictive control (MPC), rely on derivative-based optimization techniques that require explicit mathematical models. For example, necessary optimality conditions such as the Karush–Kuhn–Tucker (KKT) conditions involve differentiating the model with respect to the decision variables (Rawlings et al. 2020). However, mathematical models for bioprocesses and metabolic systems often exhibit highly nonlinear, stiff, or piecewise dynamics, posing significant differentiation challenges and potentially hindering solver convergence in model-based control approaches. Moreover, conventional MPC typically assumes deterministic system dynamics. Although stochastic MPC formulations have been proposed (Heirung et al. 2018), their practical implementation remains computationally demanding, particularly for practitioners without specialized expertise in control theory.

In contrast, our proposed RL-based approach enables the generation of robust dynamic metabolic control policies without requiring differentiation of the model with respect to decision variables, as in MPC. Instead, RL learns optimal policies by directly interacting with a simulated environment or process, which involves integrating the dynamic model forward in time; a task that can be handled in a generally efficient way using off-the-shelf numerical solvers. In our outlined method, the RL agent (or controller) determines the dynamic metabolic control policies for regulating enzyme expression by maximizing the expected value of a user-defined metric that quantifies the biosystem's production efficiency.

Additionally, our approach explicitly incorporates system uncertainties into deterministic models through domain randomization, thereby better capturing realistic bioprocess conditions and behavior. This is achieved by exposing the RL controller to varying levels of uncertainty during training, allowing it to learn policies that are not only optimal but also robust to intra- and extracellular disturbances. Moreover, domain randomization provides a systematic framework for evaluating the robustness of different dynamic metabolic control architectures *in silico*, offering a cost-effective and safe environment for early-stage decision-making in bioprocess and dynamic metabolic engineering development.

We demonstrate our approach through the dynamic metabolic control of acetyl-CoA carboxylase (ACC), a key enzyme regulating fatty acid biosynthesis in *Escherichia coli* (Ohkubo et al. 2024). Since intracellular ACC accumulation can lead to cytotoxic effects, precise dynamic modulation is essential to maintain high production efficiency and cell viability. We evaluate the robustness of our RL-derived dynamic control policies by benchmarking them against a previously optimized static metabolic control policy (Ohkubo et al. 2024) under varying levels of system uncertainty.

The remainder of this paper is structured as follows. Section 2 outlines the proposed RL-based methodology, incorporating domain randomization to derive robust dynamic metabolic control policies. Section 3 introduces the biological system used as a case study for fatty acid biosynthesis. Finally, Section 4 presents numerical results demonstrating the effectiveness and robustness of the proposed dynamic metabolic control method.

2 Robust dynamic metabolic control policies

The overall RL strategy is illustrated in Fig. 1-a. For generality, we define the system state at discrete time t as the state vector $\mathbf{x}_t \in \mathbb{R}^{n_x}$. The system evolves to the next discrete time step \mathbf{x}_{t+1} according to a Markov decision process:

$$\mathbf{x}_{t+1} = \mathbf{f}_x(\mathbf{x}_t, \mathbf{u}_t, \boldsymbol{\omega}, \mathbf{d}_t), \quad \forall t \in \{0, 1, \dots, N_x - 1\}, \quad (1)$$

where $\mathbf{f}_x : \mathbb{R}^{n_x} \times \mathbb{R}^{n_u} \times \mathbb{R}^{n_\omega} \times \mathbb{R}^{n_d} \rightarrow \mathbb{R}^{n_x}$ represents the state transition function. The variables $\mathbf{u}_t \in \mathbb{R}^{n_u}$, $\boldsymbol{\omega} \in \mathbb{R}^{n_\omega}$, and $\mathbf{d}_t \in \mathbb{R}^{n_d}$ denote the metabolic control input, constant model parameters, and stochastic disturbances of both intracellular and extracellular origin, respectively. When the disturbances follow a probability distribution $\mathcal{P}_d(\mathbf{d}_t)$, Eq. (1) describes the stochastic system dynamics. The state transition occurs over N_x time intervals, with \mathbf{x}_0 representing the initial condition.

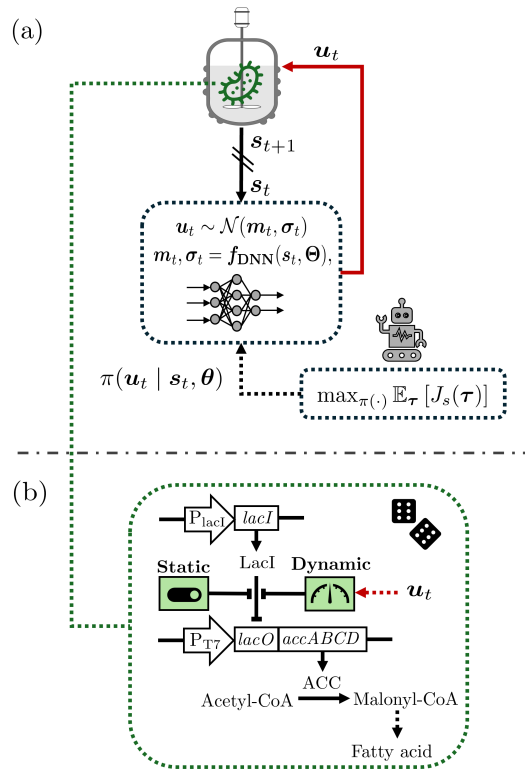


FIGURE 1 Overview of RL for generating robust dynamic metabolic control policies. (a) The core components of the RL controller and (b) the biological system under study shown.

We define a trajectory τ as the collection of states, inputs, and rewards over the entire process:

$$\tau = \{(\mathbf{x}_0, \mathbf{u}_0, R_1, \mathbf{x}_1), (\mathbf{x}_1, \mathbf{u}_1, R_2, \mathbf{x}_2), \dots, (\mathbf{x}_{N_x-1}, \mathbf{u}_{N_x-1}, R_{N_x}, \mathbf{x}_{N_x})\}, \quad (2)$$

where $R_t \in \mathbb{R}$ represents the system reward at time t , a user-defined metric that quantifies system performance in response to the applied control input.

The control input \mathbf{u}_t is sampled from a policy distribution $\pi(\cdot)$, which is conditioned on a feature vector representation of the system $\mathbf{s}_t \in \mathbb{R}^{n_s}$, providing contextual information about the system state at time t . That is:

$$\mathbf{u}_t \sim \pi(\mathbf{u}_t \mid \mathbf{s}_t, \boldsymbol{\theta}), \quad (3)$$

where $\boldsymbol{\theta} \in \mathbb{R}^{n_\theta}$ represents the policy parameters, which define the shape and properties of the policy distribution.

The conditional probability of a trajectory $\boldsymbol{\tau}$, given the policy parameters $\boldsymbol{\theta}$, is expressed as:

$$P(\boldsymbol{\tau} \mid \boldsymbol{\theta}) = P(\mathbf{x}_0) \prod_{t=0}^{N_x-1} [\pi(\mathbf{u}_t \mid \mathbf{s}_t, \boldsymbol{\theta}) P(\mathbf{x}_{t+1} \mid \mathbf{x}_t, \mathbf{u}_t)], \quad (4)$$

where $P(\mathbf{x}_0)$ represents the probability distribution of the initial state and $P(\mathbf{x}_{t+1} \mid \mathbf{x}_t, \mathbf{u}_t)$ represents the state transition probability given the current state and applied control input.

2.1 Policy gradients

The primary objective in RL is to maximize the expected system performance, represented by the return function $J_s(\boldsymbol{\tau})$, where the expectation is taken over trajectories $\boldsymbol{\tau}$ generated under the policy $\pi(\cdot)$:

$$\max_{\pi(\cdot)} \mathbb{E}_{\boldsymbol{\tau} \sim P(\boldsymbol{\tau} \mid \pi)} [J_s(\boldsymbol{\tau})]. \quad (5)$$

In the context of dynamic metabolic control, $J_s(\cdot)$ can represent key performance metrics in bioprocessing, such as the final product titer or volumetric productivity, which are common economic objectives in bioprocess optimization.

To solve the stochastic dynamic optimization problem in (5), we apply gradient ascent to iteratively update the policy parameters:

$$\boldsymbol{\theta}_{m+1} = \boldsymbol{\theta}_m + \alpha \nabla_{\boldsymbol{\theta}} \mathbb{E}_{\boldsymbol{\tau} \sim P(\boldsymbol{\tau} \mid \pi)} [J_s(\boldsymbol{\tau})]. \quad (6)$$

This update allows the policy to transition from epoch m to epoch $m + 1$ at a learning rate $\alpha \in \mathbb{R}$.

In particular, we parameterize the policy using a deep neural network (DNN), modeling it as a Gaussian distribution over the control inputs:

$$\mathbf{m}_t, \boldsymbol{\sigma}_t = \mathbf{f}_{\text{DNN}}(\mathbf{s}_t, \boldsymbol{\Theta}), \quad \mathbf{u}_t \sim \mathcal{N}(\mathbf{m}_t, \text{diag}(\boldsymbol{\sigma}_t^2)), \quad (7)$$

where $\mathbf{m}_t \in \mathbb{R}^{n_u}$ and $\boldsymbol{\sigma}_t \in \mathbb{R}^{n_u}$ denote the mean and standard deviation of the input distribution, respectively. The parameter vector $\boldsymbol{\Theta}$ represents the weights and biases of the deep neural network, thus $\boldsymbol{\theta} := \boldsymbol{\Theta}$. The control input is then sampled from the resulting Gaussian distribution. Such a stochastic control policy allows the RL agent to naturally explore (wider distributions) and exploit (narrowing of the distribution) over epochs, gradually improving the expectation in (5). It is expected that deterministic or low-uncertainty systems will result in policies with very narrow distributions, leaning toward a deterministic input.

Upon applying the Policy Gradient Theorem (Sutton et al. 1999) and incorporating Eq. (4), the gradient in Eq. (6) can be rewritten as:

$$\nabla_{\boldsymbol{\theta}} \mathbb{E}_{\boldsymbol{\tau} \sim P(\boldsymbol{\tau} \mid \pi)} [J_s(\boldsymbol{\tau})] = \int P(\boldsymbol{\tau} \mid \boldsymbol{\theta}) \nabla_{\boldsymbol{\theta}} \log P(\boldsymbol{\tau} \mid \boldsymbol{\theta}) J_s(\boldsymbol{\tau}) d\boldsymbol{\tau} = \mathbb{E}_{\boldsymbol{\tau} \sim P(\boldsymbol{\tau} \mid \pi)} \left[J_s(\boldsymbol{\tau}) \nabla_{\boldsymbol{\theta}} \sum_{t=0}^{N_x-1} \log \pi(\mathbf{u}_t \mid \mathbf{s}_t, \boldsymbol{\theta}) \right]. \quad (8)$$

The otherwise intractable expectation in the previous equation is approximated using a Monte Carlo sampling over N_{MC} sampled trajectories (or episodes) within the epoch:

$$\nabla_{\theta} \mathbb{E}_{\tau \sim P(\tau|\pi)} [J_s(\tau)] \approx \frac{1}{N_{MC}} \sum_{k=1}^{N_{MC}} \left[\frac{J(\tau^{(k)}) - \bar{J}_m(\tau)}{\sigma_{J_{sm}} + \epsilon_{mach}} \nabla_{\theta} \sum_{t=0}^{N_x-1} \log \left(\pi(\mathbf{u}_t^{(k)} | \mathbf{s}_t^{(k)}, \theta) \right) \right], \quad (9)$$

where the return function is normalized by subtracting the mean return \bar{J}_m and dividing by the standard deviation of the return values $\sigma_{J_{sm}}$ within the epoch. For numerical convenience, a small constant ϵ_{mach} is added to the denominator to prevent division by zero, particularly in cases where the system and policy become deterministic.

2.2 Domain randomization

We implement domain randomization to generate policies that are robust to system uncertainties. Rather than mechanistically or explicitly modeling all sources of uncertainty, which can be particularly challenging in biotechnological system models, we define probability distributions from which disturbances are sampled. Doing so allows the computation of the state transition in Eq. (1) under uncertainty. These probability distributions are built based on domain knowledge or empirical data. By incorporating these uncertainties during training, each Monte Carlo trajectory experiences stochastic variations, allowing the policy to generalize across a wide range of possible stochastic dynamics.

Without loss of generality, in our case study, we consider uncertainties in both the initial conditions and key model kinetic parameters. Randomization of initial conditions can be useful to capture measurement errors and variability in growth media or inoculum conditions. Similarly, randomization of kinetic parameters can be useful to capture intrinsic stochastic intracellular phenomena, external process disturbances (e.g., temperature, pH, mixing variability), or wrong/oversimplified model assumptions. Specifically, domain randomization in each Monte Carlo episode k is incorporated as follows:

$$\mathbf{x}_0^{(k)} = \mathbf{x}_0 + \mathbf{d}_x, \mathbf{d}_x \sim \mathcal{N}(\mathbf{0}, \text{diag}(\sigma_x^2)) \quad (10a)$$

$$\boldsymbol{\omega}^{(k)} = \boldsymbol{\omega}_0 + \mathbf{d}_\omega, \mathbf{d}_\omega \sim \mathcal{N}(\mathbf{0}, \text{diag}(\sigma_\omega^2)) \quad (10b)$$

where \mathbf{d}_x and \mathbf{d}_ω are normally distributed zero-mean random variables of appropriate dimensions with predefined variances σ_x^2 and σ_ω^2 , respectively. The overall disturbance vector is then defined as $\mathbf{d}_t := [\mathbf{d}_x^T, \mathbf{d}_\omega^T]^T$ (cf. Eq. (1)). Although Eqs. (10a)-(10b) assume a Gaussian distribution, alternative distributions may be used based on prior knowledge of system uncertainties.

3 Biological system

A diagram of the core engineered metabolic system considered as a case study is shown in Fig. 1-b. This system is motivated by the previous work of Ohkubo et al. (2024). Lacl is a protein constitutively expressed by the cell under the regulation of the P_{lacl} promoter. When Lacl binds to the $lacO$ sequence, it blocks the expression of the enzyme ACC (encoded by $accABCD$), regulated by the P_{T7} promoter. ACC catalyzes the conversion of acetyl-CoA to malonyl-CoA, a key intermediate in the fatty acid biosynthesis pathway.

To simulate the bioprocess for fatty acid synthesis by *E. coli* in batch fermentation regime, we consider the following dynamics for the concentrations of glucose $S \in \mathbb{R}$, cell density $X \in \mathbb{R}$, intracellular ACC $E \in \mathbb{R}$, malonyl-CoA $M \in \mathbb{R}$, Lacl $R \in \mathbb{R}$, and fatty acid $P \in \mathbb{R}$ (Ohkubo et al.

2024):

$$\frac{dS}{dt} = -\mu \cdot X, \quad (11a)$$

$$\frac{dX^*}{dt} = \mu \cdot X - \mu_d \cdot X, \quad (11b)$$

$$\frac{dE}{dt} = k_E \cdot \frac{K_{R_0}^{n_R}}{K_{R_0}^{n_R} + \left(\frac{R}{1 + \left(\frac{I}{K_I} \right)^{n_I}} \right)^{n_R}} - (d_E + \mu) \cdot E, \quad (11c)$$

$$\frac{dM}{dt} = k_M \cdot E - k_P \cdot M - \mu \cdot M, \quad (11d)$$

$$\frac{dR}{dt} = k_{R_1} - (d_R + \mu) \cdot R, \quad (11e)$$

$$\frac{dP^*}{dt} = k_P \cdot M \cdot X \cdot \left(\frac{S}{K_{S_P} + S} \right) \cdot (1 - T_P). \quad (11f)$$

$$X = H_X X^* \quad (11g)$$

$$P = H_P P^* \quad (11h)$$

$$S(t_0) = S_0, X(t_0) = X_0, E(t_0) = E_0, M(t_0) = M_0, R(t_0) = R_0, P(t_0) = P_0, \quad (11i)$$

All the dynamic states in this model are normalized and dimensionless. H_X and H_P are conversion factors in the model. H_X is dimensionless, while H_P converts the fatty acid concentration to g/L. The growth rate function μ and the toxic effects of ACC expression on biomass and product formation, represented by T_X and T_P , are governed by (Ohkubo et al. 2024):

$$\mu = k_X \cdot S \cdot (1 - T_X), \quad (12a)$$

$$T_X = T_{X_{\max}} \frac{E^{n_{T_X}}}{K_{T_X}^{n_{T_X}} + E^{n_{T_X}}}, \quad (12b)$$

$$T_P = \begin{cases} 0, & E < E_{\text{tox}} \\ \frac{(E - E_{\text{tox}})^{n_{T_P}}}{K_{T_P}^{n_{T_P}} + (E - E_{\text{tox}})^{n_{T_P}}}, & E \geq E_{\text{tox}}. \end{cases} \quad (12c)$$

Here, T_X and T_P reduce the growth rate (cf. Eq. (12a)) and the product formation rate (cf. Eq. (11f)), respectively. T_X follows Hill-type activation kinetics, while T_P is a piecewise function that follows Hill-activation kinetics once a certain enzyme expression threshold E_{tox} is reached. Therefore, it is clear that the overall system dynamics are rate-limited by both the substrate glucose and the intracellular ACC concentration. Nominal parameters and initial conditions for this model are taken from (Ohkubo et al. 2024).

It is also worth noting that the rate of enzyme expression (cf. Eq. (11c)) is influenced by the control input (inducer) denoted as $I \in \mathbb{R}$ and is assumed to come from an external source. Hereafter, for consistency of notation with Section 2, we refer to the inducer as u . Depending on the metabolic control strategy (i.e., static or dynamic), u will either remain constant throughout the process in the static approach or vary over time in the dynamic approach. In practice, the static approach can involve the use of chemical inducers, such as IPTG, which is added to the cultivation medium at a specific concentration (Ohkubo et al. 2024). When IPTG binds to Lacl, it causes Lacl to dissociate from *lacO*, resulting in the transcription of target genes. In contrast, the dynamic approach involves bidirectionally tunable inputs, which can be achieved, e.g., with the OptoLacl system (Liu et al. 2024), where Lacl is engineered to respond to light instead of IPTG. For ease of comparison, we assume that the model's parameter values hold regardless of the metabolic control strategy applied (static or dynamic).

4 Results and discussion

To assess the effectiveness of our RL-based approach for deriving robust dynamic metabolic control policies, we apply it to the biological system described in Section 3 under varying levels of uncertainty. Specifically, we introduce uncertainty levels of 0 %, 10 %, 15 %, 20 %, and 25 % in the initial conditions and in the parameters k_E and k_{R_1} (cf. Eqs. (11c) and (11e)), which regulate input-dependent ACC expression and basal LacI expression, respectively. The randomization follows the procedure outlined in Section 2.2.

The scenario with 0 % uncertainty, representing purely deterministic dynamics, serves as a reference for an ideally behaved system and initially tests the ability of our method to converge to an optimal result. For benchmarking, we compare our dynamic metabolic control approach against a static metabolic control strategy from a previous study, where an optimal constant input (IPTG concentration, μM) of $u \approx 40$ was identified (Ohkubo et al. 2024). Throughout this work, we refer to this as the *optimized static control* scenario, which serves as a baseline for evaluating the benefits of applying dynamic metabolic control.

A deep neural network with four hidden layers, each containing 20 nodes and employing LeakyReLU activation functions, was used to parameterize the policy, which was found to be sufficient for the RL implementation. The RL policy was trained in PyTorch (Paszke et al. 2019) over 350 epochs, each consisting of 500 episodes, using a learning rate of $\alpha = 0.0075$. Different values of these hyperparameters were selected to promote faster and smooth convergence. Stepwise constant inputs, applied at 1-h intervals, were used over a total process duration of 25 h, matching the time horizon of the optimized static control scenario. The feature vector s_t consisted of the two most recent state-input pairs and a process time embedding, normalized to the range $[-1, 1]$. Full state observability was assumed, as the idea of our proposed methodology is to use the dynamic mathematical model as a surrogate environment, which in principle is fully observable. We selected the final fatty acid titer as the return function to maximize, which in a batch process is equivalent to maximizing the product volumetric productivity within the given time frame. This is consistent with the objective of the optimized static control scenario.

4.1 Deterministic dynamics

Fig. 2 shows the performance of the RL-trained dynamic metabolic control system under ideal deterministic conditions (i.e., 0 % uncertainty). As expected, the return function initially exhibits a wider standard deviation across epochs while the agent explores different policies (cf. e.g. the region around epoch 25). As training progresses and the return function converges, the standard deviation decreases, indicating a shift toward exploitation mode. This demonstrates the natural balance between exploration and exploitation inherent to our RL approach based policy gradients, eliminating the need for heuristic exploration strategies.

The RL-derived dynamic metabolic control strategy follows a gradually decreasing input trend, enabling precise modulation of ACC enzyme expression. This approach rapidly accumulates ACC to extend the duration of active fatty acid production while carefully avoiding the toxicity threshold (cf. E_{tox} in Eq. (12c)). In contrast, the static control scenario leads to a slower ACC accumulation rate, delaying but ultimately failing to prevent the system from surpassing the toxicity threshold due to the irreversible nature of static induction. For other system states, LacI accumulates steadily in both static and dynamic control scenarios, as expected due to its constitutive expression. Additionally, malonyl-CoA reaches higher levels under static control because increased ACC toxicity slows down fatty acid production, reducing malonyl-CoA conversion efficiency and leading to its accumulation.

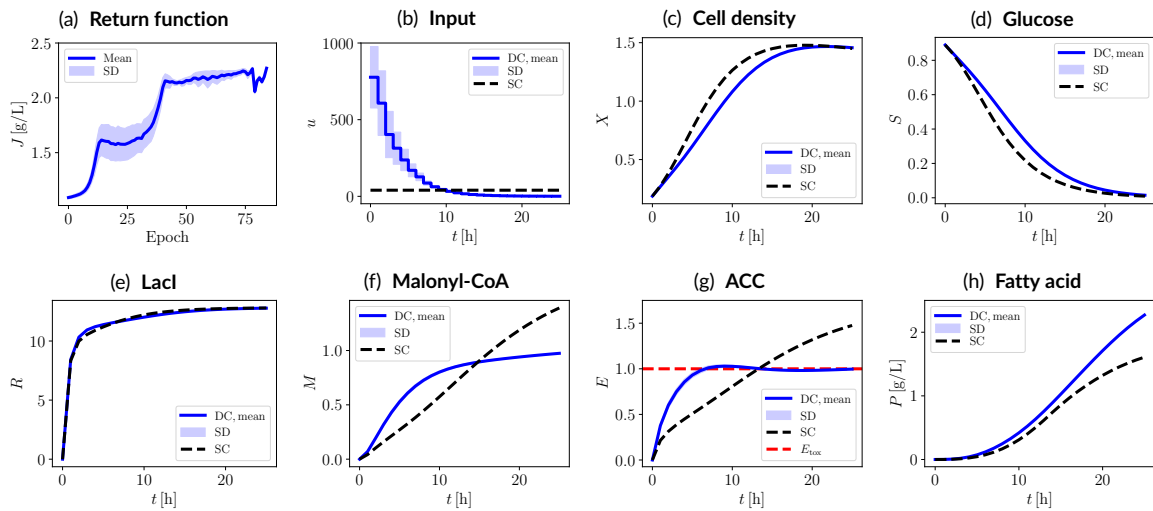


FIGURE 2 Control results under ideal conditions (i.e., no system uncertainties). (a) Evolution of the return function over epochs, up to the epoch with the highest mean value (selected control policy). The corresponding (b) input trajectory and (c)-(h) dynamic state trajectories associated with the selected control policy are also shown. The RL-derived dynamic control scenario (DC) is benchmarked against the optimized static control scenario (SC). SD: standard deviation.

As a result, the final fatty acid titer increases by approximately 41 % under dynamic control compared to static control (cf. Table 1). Thus, the RL-based dynamic policy more effectively regulates ACC expression dynamics, achieving an optimal balance between enzyme induction and its toxic effects on both cell growth and fatty acid biosynthesis, ultimately maximizing the final product titer.

TABLE 1 Summary of results.

Unc. [%]	SC [g/L]	DC [g/L]	Imp. [%]
0	1.61 ± 0.00	2.27 ± 0.00	41 %
10	1.57 ± 0.09	2.18 ± 0.20	39 %
15	1.54 ± 0.13	2.07 ± 0.31	35 %
20	1.46 ± 0.22	2.00 ± 0.39	37 %
25	1.38 ± 0.30	1.93 ± 0.45	40 %

SC: static control. DC: dynamic control. Imp.: improvement. Unc.: uncertainty level.

4.2 Policy robustness via domain randomization

The performance of the RL-derived dynamic metabolic control policies under varying levels of uncertainty is shown in Fig. 3. As expected, higher uncertainty levels lead to greater standard deviations in both the return function evolution over epochs and the dynamic states for the best-performing epoch, reflecting the increased stochasticity in the bioprocess dynamics. Despite these variations, all dynamic control scenarios under uncertainty maintain a gradually decreasing mean input trend, consistent with the deterministic case.

While the optimized trajectories exhibit larger standard deviations, the RL-derived policies successfully regulate the *mean* ACC concentration, keeping it below the toxicity threshold for fatty acid biosynthesis. However, at higher uncertainty levels (e.g., 20 % and 25 %), a slight transient overshoot is observed, yet the controller rapidly restores the mean ACC concentration to a non-toxic level. Notably, the RL-derived policy implicitly

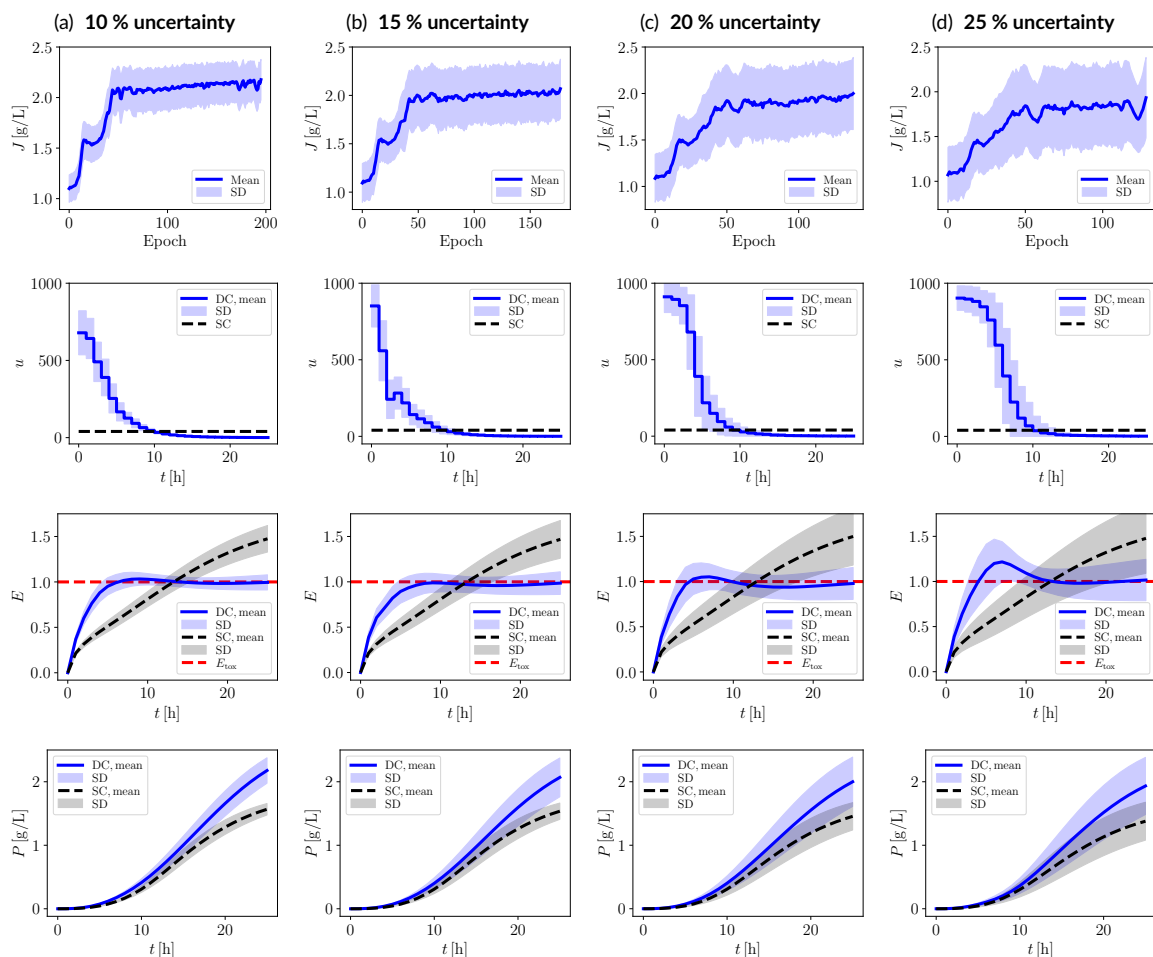


FIGURE 3 Control policies robust against system uncertainty, considering (a) 10 %, (b) 15 %, (c) 20 %, and (d) 25 % uncertainty in the initial conditions and key kinetic parameters affecting the expression of LacI and ACC. The RL-derived dynamic control scenario (DC) is benchmarked against the optimized static control scenario (SC). The return function is presented up to the epoch with the highest mean return value, matching the chosen policy. Selected dynamic state trajectories correspond to the latter policy. SD: standard deviation.

identifies the toxicity threshold, despite it being agnostic to this information *a priori*. That is, the toxicity threshold was not incorporated as a *constraint* during training. Instead, this insight emerges naturally through exploration with the surrogate environment.

Across all uncertainty scenarios, the dynamic metabolic control strategy consistently achieves mean fatty acid titer improvements of 35–40 % relative to the static control approach *under the same uncertainty conditions* (cf. Table 1). Despite this consistently significant performance gain, mean fatty acid titers exhibit a slight decline as uncertainty levels increase. This trend is expected, as higher uncertainty inevitably reduces overall system efficiency and robustness. For instance, under the highest uncertainty scenario (25 %), dynamic metabolic control performance decreases by approximately 15 % relative to the deterministic case. However, this does not undermine the value of our RL approach; rather, it demonstrates its ability to work effectively even under highly variable system conditions.

In many cases, we work with metabolic or bioprocess models derived under deterministic assumptions, modeling only the mean *for simplicity*. While this approach avoids the need to work with, e.g., stochastic dynamic differential equations, it overlooks the system's inherent uncertainty and reduces the accuracy and confidence of these models. Domain randomization allows us to incorporate this neglected stochasticity during RL training in a straightforward manner, making the control policy uncertainty-aware and enhancing its robustness. The presented results demonstrate

that our RL-derived dynamic metabolic control policies, embedded with uncertainty through domain randomization, effectively handle system uncertainties, more accurately reflecting real-world biotechnological processes.

Additionally, our strategy enables, in principle, the *in silico* evaluation of different genetic circuit topologies in terms of control efficiency and robustness. This is particularly valuable in the early stages of research and development, where identifying the most promising control topologies for experimental implementation is crucial. By providing a systematic approach to screening for robust dynamic metabolic control strategies, our method can save time and experimental resources while facilitating informed decision-making.

5 Conclusions

In this work, we proposed an RL-driven approach for deriving dynamic metabolic control policies in bioprocesses, where identifying optimal control inputs is a nontrivial task, further complicated by system uncertainties. Our method uses dynamic models as surrogate environments and introduces system uncertainties through domain randomization. This approach extends models originally designed to describe only mean dynamics by incorporating stochasticity, compensating for unmodeled uncertainties. This enables the development of robust dynamic metabolic control policies.

Our strategy provides a viable alternative to complex stochastic model-based control methods, such as stochastic MPC (Heirung et al. 2018), which can be computationally demanding and challenging to implement, particularly for non-experts in control theory. Furthermore, when dynamic models exhibit highly nonlinear, stiff dynamics or piecewise kinetic functions that introduce switch-like behavior or discontinuities, our approach offers a significant advantage. Unlike model-based control methods, which require differentiation with respect to decision variables and can be difficult to implement under the outlined model characteristics, our RL method only requires integrating the model forward in time. This makes the task generally more feasible with conventional numerical solvers. Overall, the proposed approach expands the toolbox for bioprocess optimization and control, particularly in the context of dynamic metabolic engineering under uncertainty.

Acknowledgment

SER is part of the Advanced Engineering Biology Future Science Platform (AEB FSP).

References

- Brockman, I. M., & Prather, K. L. J. (2015). Dynamic metabolic engineering: new strategies for developing responsive cell factories. *Biotechnology Journal*, 10(9), 1360–1369. doi: 10.1002/biot.201400422
- Ding, Z., Huang, Y., Yuan, H., & Dong, H. (2020). *Introduction to reinforcement learning* (H. Dong, Z. Ding, & S. Zhang, Eds.). Singapore: Springer Singapore. doi: 10.1007/978-981-15-4095-0_2
- Espinel-Ríos, S., & Avalos, J. L. (2024). Hybrid physics-informed metabolic cybergenetics: process rates augmented with machine-learning surrogates informed by flux balance analysis. *Industrial & Engineering Chemistry Research*, 63(15), 6685–6700. doi: 10.1021/acs.iecr.4c00001
- Espinel-Ríos, S., Behrendt, G., Bauer, J., Morabito, B., Pohlodek, J., Schütze, A., ... Klamt, S. (2024). Experimentally implemented dynamic optogenetic optimization of ATPase expression using knowledge-based and Gaussian-process-supported models. *Process Biochemistry*, 143, 174–185. doi: 10.1016/j.procbio.2024.04.032
- Espinel-Ríos, S., Morabito, B., Pohlodek, J., Bettenbrock, K., Klamt, S., & Findeisen, R. (2024). Toward a modeling, optimization, and predictive

- control framework for fed-batch metabolic cybergenetics. *Biotechnology and Bioengineering*, 121(1), 366–379. doi: 10.1002/bit.28575
- Glass, D. S., Jin, X., & Riedel-Kruse, I. H. (2021). Nonlinear delay differential equations and their application to modeling biological network motifs. *Nature Communications*, 12(1), 1788. doi: 10.1038/s41467-021-21700-8
- Hartline, C. J., Schmitz, A. C., Han, Y., & Zhang, F. (2021). Dynamic control in metabolic engineering: theories, tools, and applications. *Metabolic Engineering*, 63, 126–140. doi: 10.1016/j.ymben.2020.08.015
- Heirung, T. A. N., Paulson, J. A., O’Leary, J., & Mesbah, A. (2018). Stochastic model predictive control – how does it work? *Computers & Chemical Engineering*, 114, 158–170. doi: 10.1016/j.compchemeng.2017.10.026
- Hoffman, S. M., Espinel-Ríos, S., Lalwani, M. A., Kwartler, S. K., & Avalos, J. L. (2025). *Balancing doses of EL222 and light improves optogenetic induction of protein production in Komagataella phaffii*. bioRxiv. doi: 10.1101/2024.12.31.630935
- Liu, M., Li, Z., Huang, J., Yan, J., Zhao, G., & Zhang, Y. (2024). OptoLacl: optogenetically engineered lactose operon repressor Lacl responsive to light instead of IPTG. *Nucleic Acids Research*, 52(13), 8003–8016. doi: 10.1093/nar/gkae479
- Ohkubo, T., Sakumura, Y., Zhang, F., & Kunida, K. (2024). A hybrid in silico/in-cell controller that handles process-model mismatches using intracellular biosensing. *Scientific Reports*, 14(1), 27252. doi: 10.1038/s41598-024-76029-1
- Olsson, L., Rugbjerg, P., Torello Pianale, L., & Trivellin, C. (2022). Robustness: linking strain design to viable bioprocesses. *Trends in Biotechnology*, 40(8), 918–931. doi: 10.1016/j.tibtech.2022.01.004
- Oyarzún, D. A., & Chaves, M. (2015). Design of a bistable switch to control cellular uptake. *Journal of The Royal Society Interface*, 12(113), 20150618. doi: 10.1098/rsif.2015.0618
- Pal, S., & Dhar, R. (2024). Living in a noisy world—origins of gene expression noise and its impact on cellular decision-making. *FEBS Letters*, 598(14), 1673–1691. doi: 10.1002/1873-3468.14898
- Paszke, A., Gross, S., Massa, F., Lerer, A., Bradbury, J., Chanan, G., ... Chintala, S. (2019). Pytorch: an imperative style, high-performance deep learning library. In *Proceedings of the 33rd international conference on neural information processing systems*. Red Hook, NY, USA: Curran Associates Inc.
- Rawlings, J. B., Mayne, D. Q., & Diehl, M. (2020). *Model predictive control: theory, computation, and design* (2nd ed.). Santa Barbara, California: Nob Hill Publishing.
- Sutton, R. S., & Barto, A. G. (2018). *Reinforcement learning: an introduction* (2nd ed.). Cambridge, Massachusetts: The MIT Press.
- Sutton, R. S., McAllester, D., Singh, S., & Mansour, Y. (1999). Policy gradient methods for reinforcement learning with function approximation. In S. Solla, T. Leen, & K. Müller (Eds.), *Advances in neural information processing systems* (Vol. 12). MIT Press.
- Volk, M. J., Tran, V. G., Tan, S.-I., Mishra, S., Fatma, Z., Boob, A., ... Zhao, H. (2023). Metabolic engineering: methodologies and applications. *Chemical Reviews*, 123(9), 5521–5570. doi: 10.1021/acs.chemrev.2c00403
- Zhang, S., Ye, B., Chu, J., Zhuang, Y., & Guo, M. (2006). From multi-scale methodology to systems biology: to integrate strain improvement and fermentation optimization. *Journal of Chemical Technology & Biotechnology*, 81(5), 734–745. doi: 10.1002/jctb.1440

